AIAA 98-2977

Modeling of the Oscillatory Flowfield Between Two Parallel Plates with Sidewall Injection

Joseph Majdalani
Marquette University
Milwaukee, WI 53233

29th AIAA Fluid Dynamics Conference
15–18 June 1998
Albuquerque, NM

Modeling of the Oscillatory Flowfield Between Two Parallel Plates with Sidewall Injection

J. Majdalani*
Marquette University, Milwaukee, WI 53233

A mathematical model is developed for the oscillatory flowfield arising in a rectangular geometry where fluid is injected uniformly through flat, parallel and permeable walls. Linearization of the Navier-Stokes equations rests on two fundamental assumptions, namely, of a small oscillatory pressure amplitude in addition to a small injection Mach number. Field decomposition into mean and small fluctuations about the mean precedes extracting a steady, two-dimensional, rotational solution which dictates the bulk fluid motion. Time-dependent velocity decomposition into irrotational and solenoidal parts allows splitting the field into pressure and vorticity driven terms that are coupled through existing boundary conditions. Separation of variables and multiple scale expansions allow extracting an accurate, uniformly valid formulation for the rotational velocity that captures key physical elements, disclosing a nondimensional grouping that has a profound impact on the solution. Flowfield characteristics are interpreted via existing dynamic similarity parameters, including injection Strouhal and Stokes numbers. For meaningful physical settings, results are shown to agree very favorably with numerical predictions.

I. Introduction

THE focus of this paper is to derive an analytical solution to the oscillatory velocity field occurring between two porous plates in the presence of an incoming mean flow from the sidewalls. Much effort has been expended, in the past, to analyze oscillatory flows which do not include injection, or to flows which include injection yet do not exhibit any oscillatory behavior. The reader is referred to, for instance, to the work of Uchida,[1] and the references therein, where an exact solution for the pulsating viscous flow of an incompressible fluid is derived in a circular pipe, for arbitrary pressure gradients and imporous walls. Solutions to various types of steady flowfields that allow injection or suction through permeable walls are also available. See White,[2] for example, and the references therein.

The present work is unique in that it combines injection of a mean flow through permeable walls with longitudinal oscillations in a rectangular geometry. In order to achieve a solution, the Navier-Stokes equations are linearized following a fundamental assumption requiring the oscillatory pressure amplitude to be small by comparison to the mean pressure. Another restriction of a small injection Mach number through the porous walls must also be tolerated. The general procedure utilized to manage a uniformly valid solution is described below.

First, the system parameters such as geometry and principal variables are defined. The range for meaningful physical settings is addressed as well. Second, the governing equations are established along with pertinent assumptions starting with the full Navier-Stokes equations. The equations are linearized by separating the flow into a steady or mean component, and a corresponding time-dependent fluctuation (oscillatory component) that is small by comparison to the mean. Third, the solution to the steady flow component is presented in cartesian coordinates. Fourth, the unsteady flowfield is separated into two independent and linearly superimposable solutions using velocity synthesis: an irrotational and an incompressible, rotational parts. The solution to the irrotational, or so-called lamellar component of the flow, is readily identified. The rotational or so-called solenoidal component of the flow, becomes the central element in the remaining analysis. Fifth, the two-dimensional time-dependent viscous solution is formulated. The approach invokes a perturbation technique which was first introduced by the author[3] for solving flowfields in cylindrical geometries. Sixth, a comparative analysis using reliable numerical predictions is undertaken by way of verifying the accuracy associated with the final formulation.

*Assistant Professor, Department of Mechanical and Industrial Engineering. Member AIAA.

II. Problem Definition

A. Basic Geometry

The velocity field is investigated in a low aspect ratio, rectangular chamber, of length L, width W, and height $2H$ ($W >> 2H$, $L >> 2H$), where sidewall injection of a Newtonian fluid (of kinematic viscosity ν_0) occurs at a steady injection rate V_b. As represented schematically in Fig. 1, the chamber is closed at one end and attached to a choked nozzle at the downstream end (not shown). The head-end and lateral walls normal to the x axis are impenetrable. Since the chamber width is larger than its height, variations in the x direction are ignored. Fluid entering the chamber in the normal direction (y) is led to change course, swerve, and head for the nozzle. Under idealized conditions, the flow is perfectly symmetrical about the central plane, and subjected to neither swirling nor separation. Due to symmetry, the field investigation can be limited to half of the domain extending from the wall to the central plane.

In addition to the bulk fluid motion, small amplitude harmonic oscillations (of frequency ω_0 and pressure amplitude A_p) are introduced. These oscillations superimposed on the mean flow can be either externally induced or naturally occurring as a result of acoustic pressure oscillations. In cold flow experiments, a rotating valve inserted externally near the fore or aft ends,[4] a piston with a slider crank mechanism,[5] or a Scotch yoke mechanism,[6] can be used, for instance, to induce oscillatory waves traveling in the longitudinal direction that approach natural system frequencies. In combustion chambers, acoustic wave motion can be self-induced due to inherent imperfections in the combustion process which lead to wave disturbance propagation. These intrinsic disturbance waves, in turn, give rise to an internal acoustic environment. In the foregoing analysis, the physical source of oscillations will not be of concern.

B. Fundamental Assumptions

The analytical derivation to be pursued will rest upon a fundamental assumption of a low injection Mach number of $O(10^{-3})$. In cold flow experiments characterized by a typical speed of sound of about 350 m/s, a limit of 2 m/s on the injection speed must be imposed in order to satisfy the low Mach number criterion. Practically, this limit of 2 m/s is not too restrictive as, in many physical settings, it could be rather high. A second basic assumption constrains the oscillatory pressure amplitude A_p to remain small by comparison to the mean stagnation pressure p_0 at the chamber head-end. A third assumption of a constant mean pressure within the chamber will be found to be contingent upon a geometrical restriction of $L/H <$ 60. When these criteria are met, the foregoing analysis will be applicable everywhere except in the nozzle vicinity.

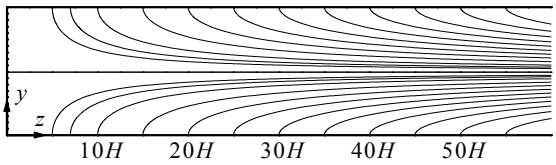

Fig. 1 Chamber geometry showing mean flow streamlines.

III. Governing Equations

A. Fundamental Equations

For constant viscosity, negligible bulk viscosity coefficient, and no body forces, the conservation of mass and momentum equations can be written as:

$$\frac{\partial \rho}{\partial t} + \nabla.(\rho \boldsymbol{u}) = 0 \tag{1}$$

$$\rho \frac{D\boldsymbol{u}}{Dt} = -\frac{\nabla p}{\gamma} + \frac{1}{Re}\left[\frac{4}{3}\nabla(\nabla.\boldsymbol{u}) - \nabla \times (\nabla \times \boldsymbol{u})\right] \tag{2}$$

where density and pressure are normalized by their mean stagnation values, ρ_0 and p_0, at the inert head-end, velocities are normalized by the speed of sound a_0, spatial coordinates are normalized by H, and time is made dimensionless by reference to the average time it takes for a pressure disturbance to travel from the porous sidewall to the centerline, (H/a_0). The Reynolds number Re in Eq. (2) is $a_0 H/\nu_0$, γ is the ratio of specific heats, and $\boldsymbol{u}(y,z,t)$ is the total velocity, including both steady and unsteady components. Determination of the latter constitutes the central purpose of this article.

B. Strategy

In what follows, the internal flowfield is decomposed into a steady and a time-dependent or oscillatory part. This is accomplished by writing each of the independent variables (pressure, density, and velocity) as a sum of their steady and time-dependent components. A small parameter perturbation scheme is justified by virtue of the original premise requiring the time-dependent part to be a small fluctuating quantity relative to its steady counterpart.[7] In order to break the analysis into digestible pieces, an assumption that must be tolerated is that the presence of time-dependent oscillations does not affect the bulk fluid motion.

Fortunately, this assumption is shown to be accurate, in detailed analyses of the mean flow solution in similar physical settings.[4,8] Since superposition of the coupled elements is sought, a detailed knowledge of the steady flowfield becomes an essential prerequisite to a successful assault on the time-dependent formulation. Equations governing both steady and time-dependent components are developed next.

C. Variable Decomposition

The total pressure can be written as the composite sum of its steady and time-dependent parts. Using asterisks to denote dimensional variables, and superscripts for perturbation orders,

$$\begin{aligned} p^* &= p^{*(0)}(y^*, z^*) + p^{*(1)}(y^*, z^*, t^*) \\ &= p^{*(0)} + A_p f(y^*, z^*)\cos(\omega_0 t^*) \end{aligned} \tag{3}$$

where the steady part of the pressure $p^{*(0)}$ will be taken to be a constant and later verified to be true. In the time-dependent part of Eq. (3), A_p represents the amplitude of the oscillatory pressure component, and f is a normalized spatial function of the order of unity. Normalizing by the mean stagnation value p_0, and using $p^{*(0)} \cong p_0$, one gets

$$p = \frac{p^{*(0)} + p^{*(1)}}{p_0} \cong 1 + \varepsilon_w f(y,z)\cos(\omega_0 t^*) \tag{4}$$

where, $\varepsilon_w = A_p / p_0$, is the gauge parameter that provides a scale to which other terms can be compared. For example, terms that are similar in size to ε_w will be described as of "first-order in ε_w." This nondimensional wave amplitude, being the smallest in magnitude, is selected as the primary perturbation parameter. Other fluctuating variables can be expanded in a similar fashion:

$$\rho(y,z,t) = \frac{\rho_0 + \rho^{*(1)}}{\rho_0} = 1 + \rho^{(1)}(y,z,t) \tag{5}$$

Velocity decomposition needs to be addressed carefully since its mean value is far from being a constant. It is proposed for now that the steady velocity will have the form $V_b \boldsymbol{U}(y,z)$, where $\boldsymbol{U}(y,z)$ is a function of $O(1)$ to be derived in Sec. IV. On that account, we expand the total dimensional velocity as

$$\boldsymbol{u}^*(y,z,t) = V_b \boldsymbol{U}(y,z) + \boldsymbol{u}^{*(1)}(y,z,t) \tag{6}$$

Normalizing by a_0, the nondimensional counterpart is found to be of the order of the injection Mach number, which represents a secondary perturbation parameter, since $\varepsilon_w < M_b << 1$. The normalized velocity becomes

$$\boldsymbol{u}(y,z,t) = M_b \boldsymbol{U}(y,z) + \boldsymbol{u}^{(1)}(y,z,t) \tag{7}$$

D. Linearized Equations

Inserting the perturbed variables in their dimensionless form into Eqs. (1)-(2), one obtains, for the zero order expansion in the wave amplitude, the set that governs the steady flow motion:

$$\nabla . \boldsymbol{U} = 0 \tag{8}$$

$$\boldsymbol{U}.\nabla \boldsymbol{U} = \frac{1}{M_b Re}\left[\frac{4}{3}\nabla(\nabla . \boldsymbol{U}) - \nabla \times (\nabla \times \boldsymbol{U})\right] \tag{9}$$

The latter can be written in a more convenient form by making use of $\boldsymbol{U}.\nabla \boldsymbol{U} = \nabla(\boldsymbol{U}.\boldsymbol{U})/2 - \boldsymbol{U} \times (\nabla \times \boldsymbol{U})$ and $\nabla \times (\nabla \times \boldsymbol{U}) = -\nabla^2 \boldsymbol{U} + \nabla(\nabla . \boldsymbol{U})$. The result is

$$\frac{1}{2}\nabla(\boldsymbol{U}.\boldsymbol{U}) - \boldsymbol{U} \times (\nabla \times \boldsymbol{U}) = \frac{1}{M_b Re}\nabla^2 \boldsymbol{U} \tag{10}$$

Collecting terms that are comparable in magnitude to the first order in the wave amplitude, the first order linearized expansion of the fundamental equations is attained (see Appendix A):

$$\partial \rho^{(1)} / \partial t + \nabla . \boldsymbol{u}^{(1)} = -M_b \nabla . (\rho^{(1)} \boldsymbol{U}) \tag{11}$$

$$\begin{aligned} \frac{\partial \boldsymbol{u}^{(1)}}{\partial t} &= M_b\left[\boldsymbol{u}^{(1)} \times (\nabla \times \boldsymbol{U}) + \boldsymbol{U} \times (\nabla \times \boldsymbol{u}^{(1)}) - \nabla(\boldsymbol{u}^{(1)}.\boldsymbol{U})\right] \\ &\quad - \frac{\nabla p^{(1)}}{\gamma} + \frac{1}{Re}\left[\frac{4}{3}\nabla(\nabla . \boldsymbol{u}^{(1)}) - \nabla \times (\nabla \times \boldsymbol{u}^{(1)})\right] \end{aligned} \tag{12}$$

Equations (11)-(12) incorporate the intricate coupling between mean and time-dependent flow components.

IV. Steady Field

A. Formulation

The current procedure follows precisely Culick's rigorous approach used to derive a similar solution in circular chambers with sidewall injection in axisymmetric, cylindrical coordinates.[9] In like fashion, we start by defining the stream function vector, $\boldsymbol{S}_f = \Psi \boldsymbol{e}_x$, and express the velocity in terms of Ψ:

$$\boldsymbol{U} = U_y \boldsymbol{e}_y + U_z \boldsymbol{e}_z = \nabla \times \boldsymbol{S}_f = \frac{\partial \Psi}{\partial z}\boldsymbol{e}_y - \frac{\partial \Psi}{\partial y}\boldsymbol{e}_z \quad (13)$$

The continuity equation being automatically satisfied by Ψ, the next step is to replace $\boldsymbol{U}$ by $\nabla \times \boldsymbol{S}_f$ in the vorticity transport equation found by taking the curl of Eq. (10). The result is an equation that does not depend on the steady pressure gradient:

$$\nabla \times \nabla\left(\frac{\boldsymbol{U}.\boldsymbol{U}}{2}\right) - \nabla \times \boldsymbol{U} \times \left(\nabla \times \boldsymbol{U}\right) = \nabla \times \frac{\nabla^2 \boldsymbol{U}}{M_b Re} \cong 0 \quad (14)$$

$$\Rightarrow \nabla \times \left(\boldsymbol{U} \times \boldsymbol{\Omega}\right) = -\left(\frac{\partial \Omega}{\partial y}\frac{\partial \Psi}{\partial z} - \frac{\partial \Omega}{\partial z}\frac{\partial \Psi}{\partial y}\right)\boldsymbol{e}_x = 0 \quad (15)$$

Since vorticity $\boldsymbol{\Omega}$ is created at the surface and carried through the chamber by convective mean flow motion in both normal and axial directions, the role played by viscous diffusion of steady vorticity remains secondary. This justifies disregarding the viscous diffusion term in the vorticity transport equation provided, of course, that the normal no-slip condition is accounted for in the derivation process. Since the primary effect of viscosity is to ensure a normal influx at the porous surface, its effect will be incorporated as part of the boundary conditions.

Using the same transformation, steady vorticity is expressible as

$$\boldsymbol{\Omega} \equiv \Omega \boldsymbol{e}_x \equiv \nabla \times \boldsymbol{U} = -\left(\frac{\partial^2 \Psi}{\partial y^2} + \frac{\partial^2 \Psi}{\partial z^2}\right)\boldsymbol{e}_x \quad (16)$$

Equations (15)-(16) show that, in order to obtain Ω and Ψ, one must solve simultaneously

$$\frac{\partial \Omega}{\partial y}\frac{\partial \Psi}{\partial z} - \frac{\partial \Omega}{\partial z}\frac{\partial \Psi}{\partial y} = 0 \quad (17)$$

$$-\Omega = \frac{\partial^2 \Psi}{\partial y^2} + \frac{\partial^2 \Psi}{\partial z^2} \quad (18)$$

By rearranging Eq. (17) and inspecting the ratio

$$\frac{\partial \Psi / \partial y}{\partial \Psi / \partial z} = \frac{\partial \Omega / \partial y}{\partial \Omega / \partial z} \quad (19)$$

it becomes apparent that the equality will stand if Ψ and Ω are directly proportional, or $\Omega = C^2 \Psi$. The value of $C = 0$ is discarded since it results in an irrotational solution that does not permit satisfying the velocity-adherence condition at $y = 0$. It can be verified that the solution desired here is possible when C is a nonzero constant. Inserting $\Omega = C^2 \Psi$ into Eq. (18), the two-dimensional Helmholtz equation is recovered:

$$\frac{\partial^2 \Psi}{\partial y^2} + \frac{\partial^2 \Psi}{\partial z^2} = -C^2 \Psi \quad (20)$$

B. The Helmholtz Solution

Letting $\Psi(y,z) = Y(y)Z(z)$, Eq. (20) can be resolved into two ordinary differential equations (ODEs) by examining

$$\frac{d^2 Y / dy^2}{Y} + C^2 = -\frac{d^2 Z / dz^2}{Z} = K_0 \quad (21)$$

These can be readily solved by careful application of four auxiliary conditions. The first requires the normal velocity U_y, and therefore $\partial \Psi / \partial z$, to be constant at the wall for steady, uniform injection; this means $-Y(0)dZ(z)/dz = \text{constant}$, or $d^2 Z(z)/dz^2 = 0$, so that, from Eq. (21), $K_0 = 0$ everywhere. For $K_0 = 0$, Eq. (21) leads to

$$\Psi(y,z) = \left(K_1 z + K_2\right)\left[K_3 \sin(Cy) + K_4 \cos(Cy)\right] \quad (22)$$

The boundary conditions are now applied: (1) The injected fluid enters normally to the surface when $U_z(0,z) = 0$, or $\partial \Psi(0,z)/\partial y = 0$, which is met only when $K_3 = 0$. (2) Symmetry about the central plane implies that $U_y(1,z) = 0$, or $\partial \Psi(1,z)/\partial z = 0$, leading to $K_1 K_4 \cos(C) = 0$, or $C = (2n+1)\pi/2$, where n is an integer. The only solution which is physically acceptable corresponds to $n = 0$. Other solutions correspond to flowfields with planes of zero U_y for $0 < y < 1$, causing internal flow reversal. When flow reversal is established, the normal flow will be directed toward the sidewall, and the axial flow will be directed toward the chamber head-end. (3) At the wall, the steady velocity component must equal V_b, hence, $U_y(0,z) = 1$, or $\partial \Psi(0,z)/\partial z = 1$, giving $K_1 K_4 = 1$. (4) Finally, the axial velocity vanishes at the chamber head-end, when $U_z(y,0) = 0$, or $Z(0)dY(y)/dy = 0$, yielding $K_2 = 0$. Substituting back into Eq. (22) gives

$$\Psi(y,z) = Y(y)Z(z) = z\cos\left(\frac{\pi}{2}y\right) \quad (23)$$

wherefrom velocity and vorticity fields are extracted by simple differentiation:

$$U_y = \cos\left(\frac{\pi}{2}y\right) \tag{24}$$

$$U_z = \frac{\pi z}{2}\sin\left(\frac{\pi}{2}y\right) \tag{25}$$

$$\boldsymbol{\Omega} = \left(\frac{\partial U_z}{\partial y} - \frac{\partial U_y}{\partial z}\right)\boldsymbol{e}_x = \frac{\pi^2}{4} z\cos\left(\frac{\pi}{2}y\right)\boldsymbol{e}_x \tag{26}$$

As one would expect, magnitudes of axial velocity and vorticity intensify in the downstream direction. Steady flow streamlines that capture the bulk fluid motion are shown in Fig 1, for several discrete values of Ψ.

C. Corrected Mean Pressure Distribution

Having determined the velocity field from the vorticity transport equation which is pressure-independent, one can use the momentum equation to deduce the pressure associated with the steady field. Therefore, without loss in generality, one can set $p(y,z,t) = 1 + p_c(y,z) + p^{(1)}(y,z,t)$, where $p_c(y,z)$ is a correction that takes into account spatial variations in pressure. A boundary condition that must be met specifies that pressure at the chamber head-end must equal (by definition) the local stagnation pressure where $p^{(0)} = 1 + p_c(1,0) = 1$, or $p_c(1,0) = 0.$ The pertinent spatially-dependent pressure correction can be obtained from Eq. (2) by direct substitution:

$$M_b \boldsymbol{U}.\nabla\left(M_b \boldsymbol{U}\right) = -\frac{\nabla p_c}{\gamma} + \frac{1}{Re}\left[\frac{4}{3}\nabla\left[\nabla.\left(M_b\boldsymbol{U}\right)\right] - \nabla\times\left[\nabla\times\left(M_b\boldsymbol{U}\right)\right]\right] \tag{27}$$

$$\Leftrightarrow \frac{\nabla p_c}{\gamma M_b^2} = -\boldsymbol{U}.\nabla\boldsymbol{U} - \frac{1}{M_b Re}\nabla\times\boldsymbol{\Omega} \tag{28}$$

which, by disregarding the smaller order term for viscous diffusion of mean vorticity, becomes

$$\nabla p_c / (\gamma M_b^2) = -\boldsymbol{U}.\nabla\boldsymbol{U} \tag{29}$$

Equation (29) can be expressed in scalar form as

$$\frac{-1}{\gamma M_b^2}\frac{\partial p_c(y,z)}{\partial y} = U_y\frac{\partial U_y}{\partial y} = \frac{1}{2}\frac{\partial\left(U_y^2\right)}{\partial y} \tag{30}$$

$$\frac{-1}{\gamma M_b^2}\frac{\partial p_c(y,z)}{\partial z} = \frac{\pi^2}{4} z\cos^2\left(\frac{\pi}{2}y\right) + \frac{1}{2}\frac{\partial\left(U_z^2\right)}{\partial z} \tag{31}$$

and integrated to obtain

$$-\frac{1}{\gamma M_b^2}p_c(y,z) = \frac{\pi^2}{8}z^2 + \frac{1}{2}\cos^2\left(\frac{\pi}{2}y\right) + \mathrm{C} \tag{32}$$

Imposing $p_c(1,0) = 0,$ the pure constant of integration is determined. It follows that the corrected steady pressure distribution must be

$$p^{(0)}(y,z) = 1 - \frac{\gamma}{2}M_b^2\left[\frac{\pi^2}{4}z^2 + \cos^2\left(\frac{\pi}{2}y\right)\right] \tag{33}$$

where the y-dependence can be safely ignored by comparison to the z-dependence, the former being of the order of a Cosine term that is squared, whereas $\pi^2 z^2$ is typically of the order of 10^3. Additionally, since M_b is of $O(10^{-3})$, and z is less than 60, the error in assuming a constant steady pressure is insignificant, being of order $M_b^2 z^2$. The corrected pressure distribution is shown in Fig. 2, indicating that axial pressure variations are indeed negligible except in long chambers with large Mach numbers. Since the Mach number in the majority of cases does not exceed 0.003, the assumption of a uniform mean value needed to represent the steady pressure distribution is fairly well justified. Having, heretofore, established the steady flowfield character, its impact on the oscillatory component is studied next.

V. Time-Dependent Field

A. Flowfield Decomposition

The notion of decomposition is made possible by virtue of an important mathematical theorem (see, for example, Lagerstrom[10]), which applies to continuous vector fields. The theorem allows a vector field to be synthesized out of two different and independent fields provided that the first is irrotational and the second is solenoidal. When applied to the time-dependent velocity vector, the statement of the theorem can be translated into an expression of the total velocity field

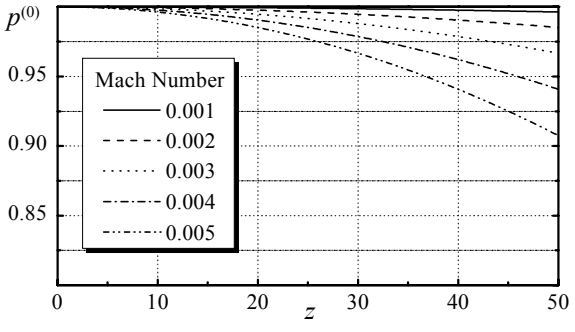

Fig. 2 Time-independent pressure component at some practical injection Mach numbers.

being a juxtaposition of two distinct components:

$$\boldsymbol{u}^{(1)} = \boldsymbol{u}_{\text{irrotational}} + \boldsymbol{u}_{\text{solenoidal}} = \hat{\boldsymbol{u}} + \tilde{\boldsymbol{u}} \tag{34}$$

provided that, in general, $\nabla \times \hat{\boldsymbol{u}} = 0$, and $\nabla \cdot \tilde{\boldsymbol{u}} = 0$. Similar decomposition of a small amplitude "disturbance" into two modes of fluctuations, a so-called pressure mode and a vorticity mode, has been accomplished previously by numerous authors, including Chu and Kovásznay,[11] Carrier and Carlson,[12], and Flandro.[13] The fundamental equations governing the unsteady disturbances to the first order in pressure wave amplitude can be written for each of the modes. The total time-dependent velocity field can be obtained thereafter by superimposing the solution vectors linearly. Denoting the irrotational (acoustic, pressure mode) component by the circumflex (^), and the solenoidal (incompressible, vortical mode) component by the tilde (~), one can express the corresponding time-dependent variables as

$$\boldsymbol{\omega}^{(1)} \equiv \nabla \times \boldsymbol{u}^{(1)} = \tilde{\boldsymbol{\omega}} \equiv \nabla \times \tilde{\boldsymbol{u}} \tag{35}$$

$$p^{(1)} = \hat{p} \tag{36}$$

$$\rho^{(1)} = \hat{\rho} \tag{37}$$

Note that vorticity is produced exclusively by the rotational mode and that pressure is caused predominantly by the irrotational pressure mode only. The so-called pseudo-pressure generated by the vortical mode is proportional to the square of the wave amplitude parameter and can be safely neglected. In actuality, both pressure and density associated with the vorticity mode can be shown to be $\tilde{p} = \tilde{\rho} = O(\varepsilon_w^2)$, or virtually insignificant.[11]

B. Splitting the Fundamental Equations

Substituting Eqs. (34)-(37) into the first order time-dependent set given by Eqs. (11)-(12), yields the following two independent sets that are coupled through existing boundary conditions.

1. Irrotational Set

$$\partial\hat{\rho}/\partial t + \nabla . \hat{\boldsymbol{u}} = -M_b \nabla . (\hat{\rho}\boldsymbol{U}) \tag{38}$$

$$\frac{\partial \hat{\boldsymbol{u}}}{\partial t} = -\frac{\nabla \hat{p}}{\gamma} - M_b\left[\nabla(\hat{\boldsymbol{u}}.\boldsymbol{U}) - \hat{\boldsymbol{u}} \times \boldsymbol{\Omega}\right] + \frac{4\nabla(\nabla . \hat{\boldsymbol{u}})}{3Re} \tag{39}$$

2. Vortical Set

$$\nabla . \tilde{\boldsymbol{u}} = 0 \tag{40}$$

$$\frac{\partial \tilde{\boldsymbol{u}}}{\partial t} = M_b\left[\tilde{\boldsymbol{u}} \times \boldsymbol{\Omega} + \boldsymbol{U} \times \tilde{\boldsymbol{\omega}} - \nabla(\tilde{\boldsymbol{u}}.\boldsymbol{U})\right] - \frac{\nabla \times \tilde{\boldsymbol{\omega}}}{Re} \tag{41}$$

C. Auxiliary Conditions

In order to determine the composite or total unsteady velocity $\boldsymbol{u}^{(1)}$, the irrotational and vortical components will have to be determined separately using the appropriate models described above. After the solutions for both parts are extracted, they must be superimposed in a manner to correctly satisfy two existing boundary conditions: Velocity adherence at the sidewall demands that the total axial velocity vanishes at $y = 0$, yielding a Dirichlet-type condition $u_z^{(1)}(0, z) = 0$, or $\tilde{u}_z(0, z) = -\hat{u}_z(0, z)$. In addition, symmetry at $y = 1$ means that $\partial u^{(1)}(1, z)/\partial y = 0$.

D. Irrotational Solution

Equations (38)-(39) exhibit a classic solution presented in most textbooks treating pressure waves and acoustics. An additional routine assumption that can be later justified is that the viscous terms in Eq. (39) are negligible. By proper manipulation of Eqs. (38)-(39), it is possible to eliminate one of the two dependent variables. The resulting second order hyperbolic partial differential equation (PDE) becomes:

$$\frac{\partial^2 \hat{p}}{\partial t^2} - \nabla^2 \hat{p} = -M_b\left[\nabla .\left(\frac{\partial \hat{p}}{\partial t}\boldsymbol{U}\right) - \gamma\nabla^2(\hat{\boldsymbol{u}}.\boldsymbol{U}) + \gamma\nabla .(\hat{\boldsymbol{u}} \times \boldsymbol{\Omega})\right] \tag{42}$$

A solution to Eq. (42) that is accurate to the first order in the Mach number is manageable by applying separation of variables and the rigid wall boundary conditions. Since our original premise requires that $H/L << 1$, the lowest naturally excited frequencies will correspond to axial oscillation modes, making it safe to neglect transverse modes of higher frequencies. In practical settings, it is always the case that chamber oscillations tend to be controlled by low oscillation modes because lower modes require less energy to excite and are encumbered by less damping than higher modes. For axial waves in a chamber with constant cross-section, a multidimensional solution reduces, conveniently, to its one-dimensional form, which is a sole function of the axial coordinate. The result for $\hat{p}(z,t)$ is expressed, for convenience, in complex variable notations with meaningful real parts:

$$\hat{p}(z,t) = \varepsilon_w \cos(k_m z)\exp(-ik_m t) \tag{43}$$

where the wave number is given by $k_m = m\pi H/L$, $m = 1, 2, 3, \ldots$, m being the mode number. The corresponding velocity can be determined

directly from the momentum conservation Eq. (39) of order M_b. The result is

$$\hat{\boldsymbol{u}}(z,t) = i\frac{\varepsilon_w}{\gamma}\sin(k_m z)\exp(-ik_m t)\boldsymbol{e}_z \tag{44}$$

E. Fundamental Vortical Equations

Using Euler's notation to express rotational velocity and vorticity components, namely,

$$\tilde{\boldsymbol{u}}(y,z,t) = \boldsymbol{V}(y,z)\exp(-ik_m t) \tag{45}$$

$$\tilde{\boldsymbol{\omega}}(y,z,t) = \boldsymbol{\varpi}(y,z)\exp(-ik_m t) \tag{46}$$

where

$$\boldsymbol{V}(y,z) = V_y\boldsymbol{e}_y + V_z\boldsymbol{e}_z \tag{47}$$

$$\boldsymbol{\varpi} = \nabla\times\boldsymbol{V} = \varpi\boldsymbol{e}_x \tag{48}$$

the vortical mass and momentum conservation equations, given by Eqs. (40)-(41) are expressed as:

$$\nabla\cdot\boldsymbol{V} = 0 \tag{49}$$

$$ik_m\boldsymbol{V} = M_b\left[\nabla(\boldsymbol{V}.\boldsymbol{U}) - \boldsymbol{V}\times\boldsymbol{\Omega} - \boldsymbol{U}\times\boldsymbol{\varpi}\right] + \frac{\nabla\times\boldsymbol{\varpi}}{Re} \tag{50}$$

Equation (50) can be further rearranged, giving

$$i\boldsymbol{V} = \sigma\left[\nabla(\boldsymbol{V}.\boldsymbol{U}) - \boldsymbol{V}\times\boldsymbol{\Omega} - \boldsymbol{U}\times\boldsymbol{\varpi}\right] + \varepsilon\nabla\times\boldsymbol{\varpi} \tag{51}$$

where

$$\sigma = \frac{M_b}{k_m} = \frac{1}{Sr} = \frac{V_b}{\omega_0 H} \sim \frac{\text{convection}}{\text{inertia}} < O(10^{-1}) \tag{52}$$

$$\varepsilon = \frac{1}{k_m Re} = \frac{1}{Re_k} = \frac{1}{2\lambda_S^2} = \left(\frac{\sqrt{\nu_0/\omega_0}}{H}\right)^2 \sim \frac{\text{diffusion}}{\text{inertia}} \sim \left(\frac{\text{hardwall Stokes layer}}{\text{characteristic length}}\right)^2 < O(10^{-4}) \tag{53}$$

are naturally arising similarity parameters representing the reciprocals of the Strouhal and kinetic Reynolds numbers, and satisfying $\varepsilon/\sigma = \nu_0/(V_b H) << 1$. Indubitably, Re_k is another form of the Stokes number, λ_S, which plays a fundamental role in oscillatory flows. Equations (49)-(51) can be expanded into

$$\frac{\partial V_y}{\partial y} + \frac{\partial V_z}{\partial z} = 0 \tag{54}$$

$$iV_y = \sigma\left[\frac{\partial}{\partial y}(V_y U_y) + U_z\frac{\partial V_y}{\partial z} + V_z\frac{\partial U_y}{\partial z}\right] - \varepsilon\left(\frac{\partial^2 V_y}{\partial z^2} - \frac{\partial^2 V_z}{\partial y\partial z}\right) \tag{55}$$

$$iV_z = \sigma\left[\frac{\partial}{\partial z}(V_z U_z) + U_y\frac{\partial V_z}{\partial y} + V_y\frac{\partial U_z}{\partial y}\right] - \varepsilon\left(\frac{\partial^2 V_z}{\partial y^2} - \frac{\partial^2 V_y}{\partial y\partial z}\right) \tag{56}$$

which reveal that closed form analytical solutions to the coupled set are not tractable without exploiting an important result that can be demonstrated numerically, and proven theoretically, only *a posteriori*. Subject to later verification, the normal vortical velocity amplitude is assumed to be of $O(M_b)$ by comparison to the axial component. Being a small quantity, ignoring V_y at the first perturbation expansion level of V will not affect the solution which, let us recall, is only accurate to the first order in the Mach number. On that account, Eq. (56) becomes

$$iV_z = \sigma\left[\frac{\partial}{\partial z}(V_z U_z) + U_y\frac{\partial V_z}{\partial y}\right] - \varepsilon\frac{\partial^2 V_z}{\partial y^2} + O(M_b) \tag{57}$$

or, equivalently,

$$iV_z = \sigma\left[\frac{\partial}{\partial z}(V_z U_z) + U_y\varpi\right] - \varepsilon\frac{\partial\varpi}{\partial y} + O(M_b) \tag{58}$$

VI. Vortical Field

A. Separation of Variables

Inserting Eqs. (24)-(25), expanding and rearranging, Eq. (57) is put into the form

$$z\frac{\partial V_z}{\partial z} = \frac{2}{\pi\sigma}\csc\left(\frac{\pi}{2}y\right)\left\{\left[i - \frac{\pi}{2}\sigma\sin\left(\frac{\pi}{2}y\right)\right]V_z - \sigma\cos\left(\frac{\pi}{2}y\right)\frac{\partial V_z}{\partial y} + \varepsilon\frac{\partial^2 V_z}{\partial y^2}\right\} \tag{59}$$

which suggests using separation of variables in order to investigate a solution of the type

$$V_z(y,z) = Y(y)Z(z) \tag{60}$$

When inserted back into Eq. (59), Eq. (60) allows splitting the original PDE into two linear ODEs, coupled through a separation constant λ_n:

$$\frac{z}{Z}\frac{dZ}{dz} = \frac{2}{\pi\sigma Y}\csc\left(\frac{\pi}{2}y\right)\left\{\left[i - \frac{\pi}{2}\sigma\sin\left(\frac{\pi}{2}y\right)\right]Y - \sigma\cos\left(\frac{\pi}{2}y\right)\frac{dY}{dy} + \varepsilon\frac{d^2Y}{dy^2}\right\} = \lambda_n \tag{61}$$

where λ_n must be strictly positive for a nontrivial outcome. For every λ_n, a solution Z_n and Y_n must be obtained. Integration of the axially dependent equation is straightforward. The exact result is $Z_n(z) = c_n z^{\lambda_n}$, where c_n is an integration constant associated with λ_n. Since the governing equation is linear, any linear combination of two or more solutions is also a solution, and one can write, in general, for all possible λ_n

$$V_z(y,z) = \sum_{\lambda_n} c_n z^{\lambda_n} Y_n(y) \tag{62}$$

where λ_n must be determined from the no-slip boundary condition at the wall giving rise to the strong coupling between pressure and vorticity modes. As a consequence, rotational and irrotational components of the axial velocity cancel out at $y = 0$. This is achieved when, $\tilde{\boldsymbol{u}}_z = -\hat{\boldsymbol{u}}_z$, or

$$V_z(0,z) = -(\varepsilon_w/\gamma)i\sin(k_m z) \tag{63}$$

Inserting Eq. (63) into Eq. (62), writing out the MacLaurin series expansion for the Sine function, and equating summation terms yields

$$\sum_{\lambda_n} c_n z^{\lambda_n} Y_n(0) \equiv -\frac{\varepsilon_w}{\gamma} i\sum_{n=0}^{\infty}\frac{(-1)^n (k_m z)^{2n+1}}{(2n+1)!} \tag{64}$$

which holds true when $\lambda_n = 2n+1, n = 0,1,\ldots$, and

$$c_n = -\frac{\varepsilon_w}{\gamma} i\frac{(-1)^n (k_m)^{2n+1}}{(2n+1)!} \tag{65}$$

$$Y_n(0) = 1 \tag{66}$$

turning Eq. (62) into

$$V_z(y,z) = -\frac{\varepsilon_w}{\gamma} i\sum_{n=0}^{\infty}\frac{(-1)^n (k_m z)^{2n+1}}{(2n+1)!} Y_n(y) \tag{67}$$

In order to satisfy Eq. (61), the velocity eigenfunction $Y_n(y)$ is left to be determined from

$$\varepsilon\frac{d^2Y_n}{dy^2} - \sigma\cos\left(\frac{\pi}{2}y\right)\frac{dY_n}{dy} + \left[i - \frac{\pi}{2}\sigma(1+\lambda_n)\sin\left(\frac{\pi}{2}y\right)\right]Y_n = 0 \tag{68}$$

which is subjected to the two naturally occurring boundary conditions:

$$Y_n(0) = 1 \text{ (no-slip condition)} \tag{69}$$

$$\frac{dY_n(1)}{dy} = 0 \text{ (axial symmetry)} \tag{70}$$

Integration here is not straightforward. If a direct analytical solution to Eqs. (68)-(70) was possible, $V_n(y,z)$ would have been exactly determined. The inherent difficulty in integrating Eq. (68) stems from the existing variable coefficients which, unless linearized, do not permit an exact solution. Due to an ostentatious logarithmic singularity at $y = 1$, conventional perturbative tools are futile in treating Eq. (68), which eludes matched asymptotic, WKB, and standard multiple-scale expansions. Achieving a uniformly valid analytical solution takes much effort, as shown by Majdalani.[14] Based on a variant, two-variable, multiple-scale expansion procedure, this closed form expression for Y_n is

$$Y_n(y) = \left[\cos\left(\frac{\pi}{2}y\right)\right]^{(1+\lambda_n)} \exp\left\{-\xi\sec^3\left(\frac{\pi}{2}y\right)\eta(y) + \frac{\pi^2}{4}\xi\sigma^2(1+\lambda_n)\sec\left(\frac{\pi}{2}y\right)\eta(y)\left[\lambda_n\tan^2\left(\frac{\pi}{2}y\right) - 1\right] - i\pi\xi\sigma\left(\frac{1}{2}+\lambda_n\right)\eta(y)\sec^2\left(\frac{\pi}{2}y\right)\tan\left(\frac{\pi}{2}y\right) + \frac{2i}{\pi\sigma}\ln\tan\left[\frac{\pi}{4}(1+y)\right]\right\} + O(\varepsilon) \tag{71}$$

where $\xi = \varepsilon/\sigma^3$, $\eta(y) = y\left[1 + cy^c\left(y\hat{y}^{-1} - c\ln\hat{y}\right)\right]^{-1}$, $\hat{y} = 1 - y$, and $c = 3/2$.

B. Infinite Series Solution

Substituting Eq. (71) into Eq. (67), letting $\theta = \pi y/2$, and summing up over all λ_n gives

$$V_z(y,z) = -\frac{\varepsilon_w}{\gamma} i \sum_{n=0}^{\infty} \frac{(-1)^n (k_m z)^{2n+1}}{(2n+1)!} (\cos\theta)^{(2n+2)}$$
$$\times \exp\left[-\xi \frac{\eta(y)}{\cos^3\theta} + \xi\sigma^2 \frac{\pi^2 \eta(y)}{4\cos\theta} (1+\lambda_n)(\lambda_n \tan^2\theta - 1) \right.$$
$$\left. + \frac{2i}{\pi\sigma} \ln\tan\left(\frac{\theta}{2}+\frac{\pi}{4}\right) - i\pi\xi\sigma\left(\frac{1}{2}+\lambda_n\right)\eta(y)\sec^2\theta\tan\theta \right]$$
$$+ O(\varepsilon) \qquad (72)$$

From Eq. (45), $\tilde{u}_z$ can be written in an infinite series form as well. Regrouping and invoking elementary trigonometric identities, $\tilde{u}_z$ can be expressed in a form that clearly displays the leading order terms and smaller terms of $O(\sigma^2)$:

$$\tilde{u}_z(y,z,t) = -\frac{\varepsilon_w}{\gamma} i\cos\theta \sum_{n=0}^{\infty} \frac{(-1)^n (k_m z\cos\theta)^{2n+1}}{(2n+1)!} \times$$
$$\exp\left(\frac{-\xi\eta}{\sec^3\theta} \left\{ 1 + \frac{\pi^2\sigma^2}{4}(1+\lambda_n)\left[\cos 2\theta + (1-\lambda_n)\sin^2\theta\right] \right\} \right.$$
$$\left. + \frac{i}{\sigma}\left[\frac{2}{\pi}\ln\tan\left(\frac{\theta}{2}+\frac{\pi}{4}\right) - \pi\xi\sigma^2\left(\frac{1}{2}+\lambda_n\right)\frac{\eta\sin\theta}{\cos^3\theta} \right] - ik_m t \right)$$
$$+ O(\varepsilon) \qquad (73)$$

Fortunately, Eq. (73) is a rapidly converging series.

C. Closed Form Solution

Analyzing Eq. (73) carefully shows that it can be written in a closed form by ignoring terms that are much smaller than the order of precision associated with the infinite series itself for the range of physically meaningful settings. The result is, for all practical purposes, an equivalent closed form expression that carries many advantages:

$$\tilde{u}_z(y,z,t) = -\frac{\varepsilon_w}{\gamma} i\cos\theta \sin(k_m z\cos\theta)$$
$$\times \exp\left[\frac{-\xi\eta}{\sec^3\theta}\left(1 + \frac{\pi^2\sigma^2}{2}\cos 2\theta \right) + \frac{2i}{\pi\sigma}\ln\tan\left(\frac{\theta}{2}+\frac{\pi}{4}\right) \right.$$
$$\left. - i\frac{3\pi}{2}\xi\sigma\eta\sec^2\theta\tan\theta - ik_m t \right] \qquad (74)$$

For instance, Eq. (74) can be expressed in a compact form in terms of a spatial damping function ζ and a spatial phase angle Φ, each of which written out as a leading-order term followed by a small first-order correction:

$$\tilde{u}_z = -\frac{\varepsilon_w}{\gamma} i\cos\theta \sin(k_m z\cos\theta) \exp\zeta \exp\left[-i(k_m t + \Phi)\right] \qquad (75)$$

where

$$\zeta = \zeta_0 + \zeta_1, \quad \Phi = \Phi_0 + \Phi_1 \qquad (76)$$

$$\zeta_0 = -\xi\eta\sec^3\theta, \quad \Phi_0 = -\frac{2}{\pi\sigma}\ln\tan\left(\frac{\theta}{2}+\frac{\pi}{4}\right) \qquad (77)$$

$$\zeta_1 = -\xi\sigma^2\pi^2\frac{\eta\cos 2\theta}{2\cos^3\theta}, \quad \Phi_1 = \pi\xi\sigma\frac{3\eta\sin\theta}{2\cos^3\theta} \qquad (78)$$

D. Reduced Closed Form Solution

Equation (75) can be further simplified by neglecting terms of $O(\sigma^2)$ and smaller (i.e., ζ_1 and Φ_1). The remarkably reduced expression is found to match both numerical and infinite series results with a margin of error that is smaller than M_b. Since there is no need to be more accurate than Eq. (57) itself which ignores the normal velocity component of order M_b, a practical expression is made available by retaining the leading order terms in the spatial damping and phase functions. A short and accurate rotational solution ensues

$$\tilde{u}_z(y,z,t) = -\frac{\varepsilon_w}{\gamma} i\cos\theta \sin(k_m z\cos\theta)$$
$$\times \exp\left[-\frac{\xi\eta}{\cos^3\theta} + \frac{2i}{\pi\sigma}\ln\tan\left(\frac{\theta}{2}+\frac{\pi}{4}\right) - ik_m t \right] \qquad (79)$$

which can be written in an elegant form, in terms of the steady flow stream function and normal velocity:

$$\tilde{u}_z(y,z,t) = -\frac{\varepsilon_w}{\gamma} iU_y \sin(k_m \Psi)$$
$$\times \exp\left\{ -\xi\frac{\eta}{U_y^3} - i\left[k_m t - \frac{2}{\pi\sigma}\ln\tan\left(\frac{\theta}{2}+\frac{\pi}{4}\right) \right] \right\} \qquad (80)$$

When the irrotational velocity component is added to $\tilde{u}_z$ in Eq. (34), a solution for $\boldsymbol{u}^{(1)}$ is achieved to $O(M_b)$. The depth of penetration of the resulting time-dependent velocity can be determined using either one of the three analytical versions represented by Eqs. (73)-(75), of theoretically decreasing accuracy. A reliable numerical solution to Eq. (57) can also be achieved using a Runge-Kutta scheme of order seven.[15] When results are overlaid in Fig. 3, differences are found to be visually indiscernible, except for very large σ and small ε (corresponding to unrealistic physical settings), where a hardly perceptible discrepancy is seen to exist between the reduced closed form solution and

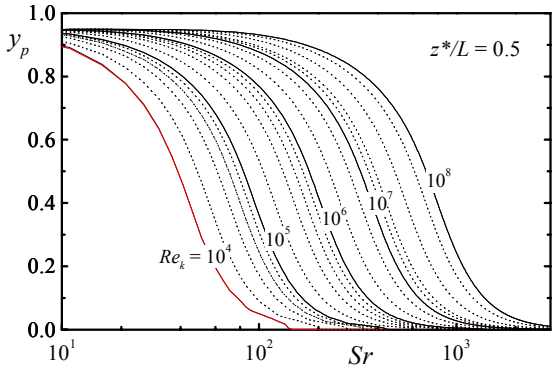

Fig. 3 Virtually indistinguishable results for the boundary-layer thickness at one axial station predicted from infinite series, closed form, and reduced closed form expressions, corresponding to Eqs. (73), (74), and (80).

all others. In addition to its simplicity and remarkable precision, Eq. (80) reveals the leading-order terms which seem to influence the solution. This allows identifying the physical phenomena of most significance to be the convection of unsteady vorticity by the mean flow (in both axial and normal directions), unsteady inertia, and viscous diffusion of unsteady vorticity. As could be extrapolated from Fig. 3, Eq. (80) concurs with numerical and infinite series predictions remarkably well.

E. Normal Velocity

Having determined $\tilde{u}_z$, the normal component $\tilde{u}_y$ can be derived analytically from Eq. (40) for mass conservation. To begin, we propose an *ansatz* of the form

$$\tilde{u}_y = \frac{\varepsilon_w}{\gamma} G(y) \cos(k_m z \cos\theta) \exp\zeta \exp\left[-i(k_m t + \Phi)\right] \tag{81}$$

where $G(y)$ must be determined to satisfy continuity. Substituting Eq. (75) and Eq. (81) into Eq. (40), the spatial function $G(y)$ that leads to a balance between highest order quantities is extracted in order to ensure that $\partial\tilde{u}_y/\partial y \equiv -\partial\tilde{u}_z/\partial z$ is satisfied in the leading order terms. This occurs when

$$G(y) = M_b U_y^3 \tag{82}$$

leading to

$$\tilde{u}_y = \frac{\varepsilon_w}{\gamma} M_b U_y^3 \cos(k_m \Psi) \exp\zeta \exp\left[-i(k_m t + \Phi)\right] \tag{83}$$

which indicates that the original assumption of $\tilde{u}_y/\tilde{u}_z = O(M_b)$ —that led to Eq. (57)— is truly justifiable.

VII. Solution Characteristics

A. Total Time-Dependent Velocity

Since $\hat{u}_y = 0$, the total unsteady, normal velocity component is $u_y^{(1)} = \tilde{u}_y$. From Eq. (34), $u_z^{(1)}$ can be constructed by combining rotational and irrotational components:

$$u_z^{(1)}(y,z,t) = \frac{\varepsilon_w}{\gamma} i\left\{\sin(k_m z)\exp(-ik_m t) - \cos\theta \sin(k_m z\cos\theta)\exp\left[\zeta - i(k_m t + \Phi)\right]\right\} \tag{84}$$

or, equivalently, in the real domain,

$$u_z^{(1)}(y,z,t) = \frac{\varepsilon_w}{\gamma}\left[\overbrace{\sin(k_m z)\sin(k_m t)}^{\text{irrotational part}} - \overbrace{\underbrace{\cos\theta \sin(k_m z\cos\theta)\exp\zeta}_{\text{rotational wave amplitude}}\ \underbrace{\sin(k_m t + \Phi)}_{\text{wave propagation}}}^{\text{rotational part}}\right] \tag{85}$$

Evidently, $u^{(1)}$ is prescribed by $u_z^{(1)}$ which is a harmonic wave —traveling in the positive y direction— characterized by a wave amplitude that diminishes exponentially with increasing distance from the sidewall. The vortical wave amplitude is actually controlled by two terms: an exponentially decaying term, made possible by inclusion of viscous dissipation, that decreases with the distance from the wall, and a sinusoidal term, made possible by inclusion of axial mean flow convection of unsteady vorticity, which varies harmonically with the distance from the head-end, and also decreases with the distance from the wall. By inspection of the spatial damping function ζ in Eq. (75) and Eq. (85), increasing viscosity is found to cause the rotational wave to decay more rapidly, preventing a deeper inward penetration of vorticity. This effect is contrary to the boundary-layer "thickening" role played by viscosity in oscillatory flows between parallel walls in the absence of injection. Incorporation of injection appears to alter the flow character quite dramatically. Results from Eq. (85) are congruent with numerical predictions which are achieved with a high order of accuracy (using a nine-stage Runge-Kutta scheme, and a step size of 10^{-6}, with an associated global error of order seven).[15] This agreement shown in Fig. 4 causes graphical results to become visually indiscernible.

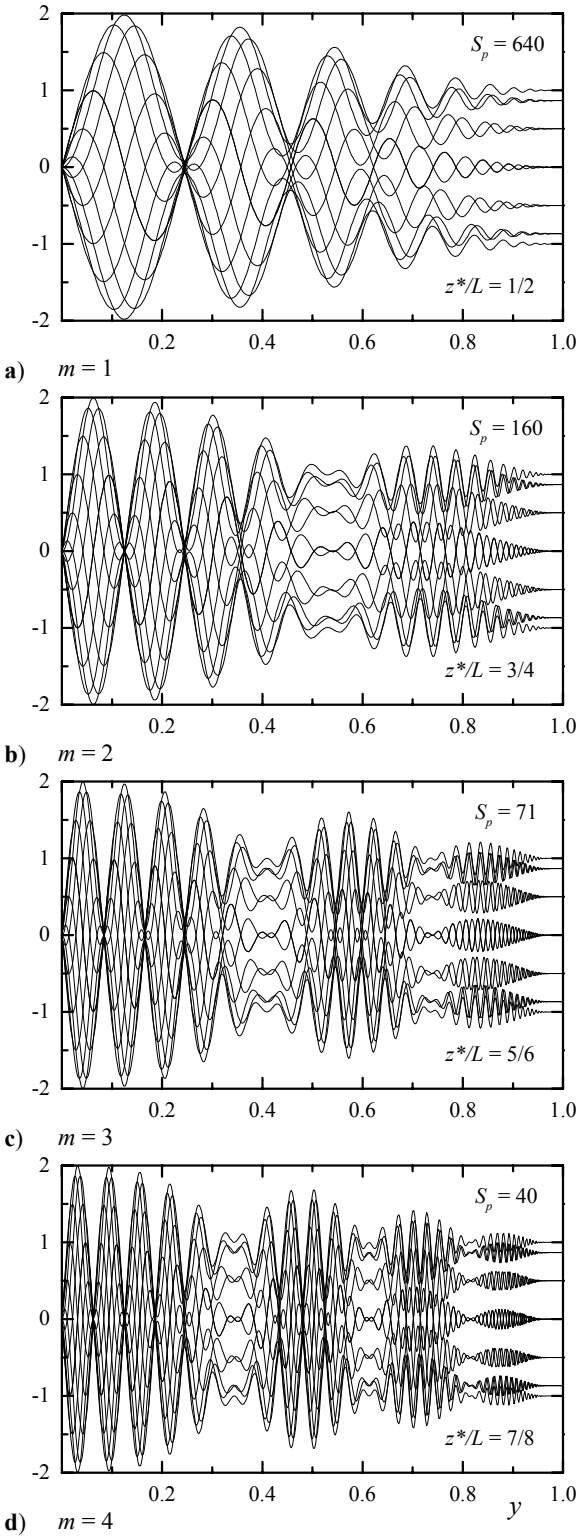

Fig. 4 Evolution of unsteady velocity obtained numerically and analytically (indiscernible) when overlaid at 12 evenly spaced times in a typical chamber. Results are for the first four oscillation modes evaluated at the last pressure node.

When, in Fig. 4, numerical and analytical velocity distributions are overlaid at 12 evenly spaced times, only 12 lines are perceived. Velocity time evolutions shown correspond to a full oscillation cycle and the first four pressure oscillation modes. The profiles are displayed at key axial positions corresponding to the location from the head-end of the last harmonic pressure node.

A key feature captured very well by the analytical solution is that of the rotational velocity amplitude vanishing m times at the m^{th} pressure node. As shown in Figs. 4b-d, the rotational amplitude decays prematurely to zero somewhere between the wall and the central plane, corresponding to lines of zero unsteady vorticity. This peculiar effect, which is attributable to the mean flow, downstream convection of zero unsteady vorticity lines, is further evidence that the influence of the mean flow on the time-dependent field has been correctly incorporated.

B. Wave Propagation Speed

The normal speed of propagation of rotational waves can be determined to be equal to the steady flow velocity ($V_b U_y$) from the wave propagation term in Eq. (85). As a result, the normalized spatial wavelength is calculated to be ($2\pi U_y / Sr$). This explains the progressively larger number of reversals per unit distance for a fluid traveling away from the wall. For pressure oscillations at the fundamental mode, velocity shape profiles are shown in Fig. 5 at various axial locations for typical Re_k and Sr values. As anticipated, the normal wavelength diminishes at higher Sr or frequencies. In addition, time-dependent rotational effects become more pronounced in the downstream direction where time-dependent vorticity permeates the field.

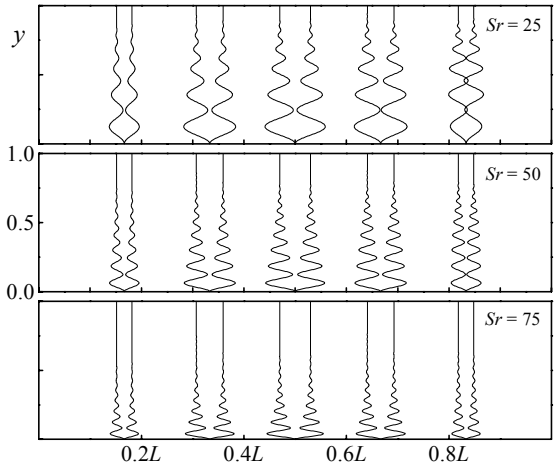

Fig. 5 Outer envelope of time-dependent velocity shown at five axial locations for $Re_k = 10^5$.

C. Total Time-Dependent Vorticity

By differentiating $\tilde{u}_z$, total unsteady vorticity is found to depend directly on the Strouhal number

$$\boldsymbol{\omega}^{(1)} = \frac{\varepsilon_w}{\gamma} Sr \sin\left(k_m z U_y\right) \exp\zeta \cos\left(k_m t + \Phi\right) \boldsymbol{e}_x \quad (86)$$

The vorticity amplitude is largest near the wall where it is generated by the oscillatory pressure gradient normal to mean flow streamlines. Moving away from the wall, vorticity diminishes, primarily, because of the downstream convection of $\boldsymbol{\omega}^{(1)}$ by U_z and the inward decrease in U_y, both aided by viscous diffusion. As with velocity, vorticity amplitudes depreciate more rapidly at lower injection speeds, and at higher frequencies and kinematic viscosities. Higher injection causes vorticity to last longer, reach deeper, and permeate larger domains above the wall.

D. Boundary-Layer Thickness

In general, the boundary-layer thickness will depend on the rate of decay of the wave amplitude. The wave amplitude that controls the evolution of the outer envelope of the rotational velocity can be expressed, to $O(M_b)$, as

$$\left\|\tilde{u}^{(1)}\right\| = \frac{\varepsilon_w}{\gamma} \cos\left(\frac{\pi}{2} y\right) \sin\left[k_m z \cos\left(\frac{\pi}{2} y\right)\right] \times \exp\left[-\frac{\eta(y)}{S_p} \sec^3\left(\frac{\pi}{2} y\right)\right] \quad (87)$$

Since the point above the wall where this amplitude becomes $\alpha \equiv 1\%$ of its irrotational counterpart is habitually defined to be the edge of the boundary layer region, it follows that the depth of penetration y_p extending from the wall to the edge of the boundary layer must be calculated by finding the root of

$$\cos\left(\frac{\pi}{2} y_p\right) \sin\left[k_m z \cos\left(\frac{\pi}{2} y_p\right)\right] \times \exp\left[-\frac{\eta(y_p)}{S_p} \sec^3\left(\frac{\pi}{2} y_p\right)\right] - \alpha \left|\sin\left(k_m z\right)\right| = 0 \quad (88)$$

Plots of y_p versus Sr for a wide range of Re_k are shown in Fig. 6 at two axial stations. The wide spread in the data makes it difficult to interpret the dependence of y_p on actual physical parameters. This problem is alleviated by referring to Eq. (88) which clearly shows that the term involving exponential boundary layer decay is a strong function of the penetration number, $S_p = \xi^{-1}$. This subtle realization motivates generating curves of y_p versus S_p, for wide variations in Re_k and Sr. As shown in Fig. 7, entire families of curves, such as those shown in Fig. 3 and Fig. 6 at discrete axial stations, collapse splendidly into single curves per axial location. This significant result reveals that y_p does not depend on Re_k and Sr separately, but rather on $S_p = V_b^3 / (\omega_0^2 \nu_0 H)$, a key similarity parameter that resembles, in importance, the Stokes number in oscillating flows over nontranspiring walls. Unlike many similarity parameters, S_p cannot be disclosed by standard dimensional analysis, no matter how parameters are selected.

Figure 7 brings into focus the character of the oscillatory boundary layer over permeable walls. For instance, it is clear that y_p depends on the penetration and pressure mode numbers, and, to a lesser degree, on the axial station within the chamber. For small penetration numbers, the penetration depth varies linearly with S_p, independently of z. The larger the

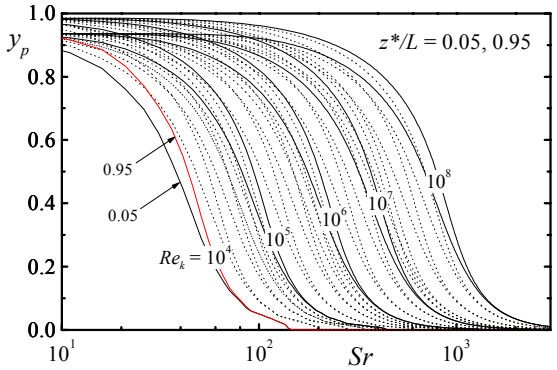

Fig. 6 Locus of the oscillatory boundary-layer thickness at two axial stations.

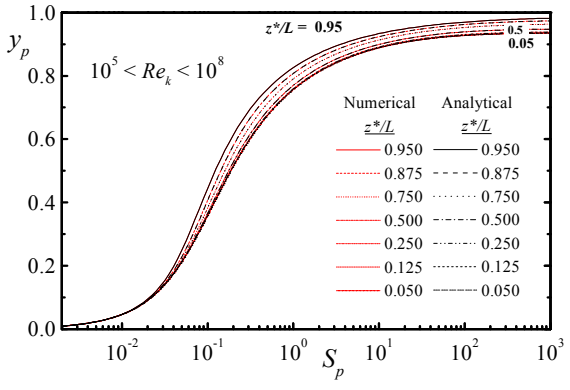

Fig. 7 The boundary-layer thickness determined numerically and analytically (indiscernible) at seven discrete axial locations.

penetration number, the larger the penetration depth will be due to a smaller argument in the exponentially decaying term. In addition, increasing the injection speed, or decreasing viscosity, frequency, or chamber height enhances the depth of penetration. Eventually, for sufficiently large S_p, y_p tends asymptotically to a maximum fixed value per axial position.

In order to pinpoint this maximum possible penetration depth, y_{pm}, occurring per axial station and mode number, we realize that, for the same geometry and injection speed, larger penetration occurs in fluids with smaller viscosity. In the ideal case of zero viscosity, rotational waves face minimum friction and, thereby, travel the furthest distance from the wall. The asymptotic limit on the thickness of the boundary layer can thus be determined from the inviscid formulation of the penetration depth —which only depends on the axial station and pressure mode. From Eq. (88), we get

$$\cos\left(\frac{\pi}{2}y_{pm}\right)\sin\left[k_m z\cos\left(\frac{\pi}{2}y_{pm}\right)\right]-\alpha\left|\sin(k_m z)\right|=0 \quad (89)$$

which must be first expressed in terms of $\hat{y}_{pm}=1-y_{pm}$ for an asymptotic expansion in small $\hat{y}_{pm}$ to be manageable. The resulting expansion formula is

$$y_{pm}=1-\frac{2}{\pi}\sqrt{\alpha\frac{\left|\sin(k_m z)\right|}{k_m z}}+O\left(\hat{y}_{pm}{}^3\right) \quad (90)$$

which allows predicting the inviscid depth of penetration quite accurately. A maximum truncation error of 2.62×10^{-4} corresponds to the largest value of $\hat{y}_{pm}$, which is 0.0636 for $z=0$. Since the maximum truncation error is about an order of magnitude smaller than M_b, Eq. (90) can be exchanged for the numerical solution to Eq. (89). This is illustrated in Fig. 8 below for the first four pressure modes.

VIII. Conclusions

In this paper, a clear analytical formulation is managed for the oscillatory flowfield with sidewall injection when the ratio of the oscillatory pressure amplitude to the mean pressure amplitude is small by comparison to the mean injection Mach number (i.e., by one order of magnitude or less). Closed form analytic expressions describing the character of the resulting boundary layer are furnished to elucidate the peculiar features of the oscillatory "Stokes" layer with injection in a rectangular geometry. The latter is found to exhibit a strong dependence on a nondimensional grouping that eliminates one dynamic similarity parameter and facilitates data correlation and interpretation. This so-called penetration number, $S_p=V_b^3/(\omega_0^2\nu_0 H)$, plays a similar role to the well-known Stokes number, $\lambda_S=H\sqrt{\omega_0/(2\nu_0)}$, encountered in the analyses of oscillatory flows over impenetrable walls. Unlike the Stokes number, however, the boundary layer grows larger at higher S_p, corresponding to smaller viscosities. In all cases, increasing the frequency or the distance separating the sidewalls reduces the nondimensional boundary layer thickness. The penetration depth is larger at higher injection rates since rotational effects established near the wall are felt deeper into the field when carried away more intensely by the normal component of the incoming mean flow. In retrospect, the axial location measured from the head end is relevant as well, especially in long chambers or at high oscillation modes. In any event, four mechanisms are identified to be the most appreciable in altering the flowfield character; these include, first and foremost, the convection of unsteady vorticity by the mean flow in both the normal and axial directions; equal in importance is the inertia associated with harmonic oscillations; and, finally, the viscous dissipation of unsteady vorticity which has a profound effect on the rate of decay of the rotational region, and

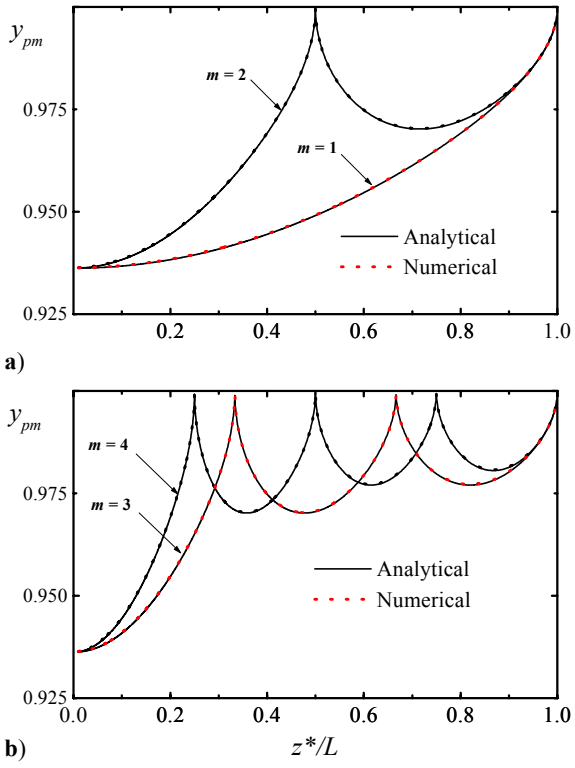

Fig. 8 Trace of the maximum boundary-layer thickness for ideal fluids shown for the first four oscillation modes: (a) *m* = 1, 2 and (b) *m* = 3, 4.

which must not be ignored if an accurate prediction of the flowfield behavior is desired away from the wall.

Appendix A: Linearization Details

Inserting the expanded variables into Eq. (1) yields

$$\partial\left(1+\rho^{(1)}\right)/\partial t+\nabla.\left[\left(1+\rho^{(1)}\right)\left(M_b\boldsymbol{U}+\boldsymbol{u}^{(1)}\right)\right]=0 \quad \text{(A1)}$$

$$\nabla.\left(M_b\underbrace{\boldsymbol{U}}_{O(\varepsilon_w^0)}+\underbrace{\boldsymbol{u}^{(1)}}_{O(\varepsilon_w^1)}+M_b\underbrace{\rho^{(1)}\boldsymbol{U}}_{O(\varepsilon_w^1)}+\underbrace{\rho^{(1)}\boldsymbol{u}^{(1)}}_{O(\varepsilon_w^2)}\right)+\partial\rho^{(1)}/\partial t=0 \quad \text{(A2)}$$

Collecting terms to the first order in the wave amplitude, and neglecting smaller terms, one gets

$$\partial\rho^{(1)}/\partial t+\nabla.\left(\boldsymbol{u}^{(1)}+\rho^{(1)}M_b\boldsymbol{U}\right)=0 \quad \text{(A3)}$$

which is Eq. (11). Inserting the expanded variables into Eq. (2), and recalling that $\nabla\cdot\boldsymbol{U}=0$, we get

$$\rho\partial\boldsymbol{u}/\partial t=\left(1+\rho^{(1)}\right)\partial\left(M_b\boldsymbol{U}+\boldsymbol{u}^{(1)}\right)/\partial t=\partial\boldsymbol{u}^{(1)}/\partial t+\rho^{(1)}\partial\boldsymbol{u}^{(1)}/\partial t \quad \text{(A4a)}$$

$$\boldsymbol{u}.\nabla\boldsymbol{u}=\left(M_b\boldsymbol{U}+\boldsymbol{u}^{(1)}\right).\nabla\left(M_b\boldsymbol{U}+\boldsymbol{u}^{(1)}\right)=M_b^2\boldsymbol{U}.\nabla\boldsymbol{U}+M_b\boldsymbol{U}.\nabla\boldsymbol{u}^{(1)}+M_b\boldsymbol{u}^{(1)}.\nabla\boldsymbol{U}+\boldsymbol{u}^{(1)}.\nabla\boldsymbol{u}^{(1)} \quad \text{(A4b)}$$

$$\rho\boldsymbol{u}.\nabla\boldsymbol{u}=\left(1+\rho^{(1)}\right)\boldsymbol{u}.\nabla\boldsymbol{u}=M_b^2\boldsymbol{U}.\nabla\boldsymbol{U}+M_b\boldsymbol{U}.\nabla\boldsymbol{u}^{(1)}+M_b\rho^{(1)}\boldsymbol{u}^{(1)}.\nabla\boldsymbol{U}+M_b^2\rho^{(1)}\boldsymbol{U}.\nabla\boldsymbol{U}+\rho^{(1)}\boldsymbol{u}^{(1)}.\nabla\boldsymbol{u}^{(1)}+M_b\boldsymbol{u}^{(1)}.\nabla\boldsymbol{U}+\boldsymbol{u}^{(1)}.\nabla\boldsymbol{u}^{(1)}+M_b\rho^{(1)}\boldsymbol{U}.\nabla\boldsymbol{u}^{(1)} \quad \text{(A4c)}$$

$$-\nabla p/\gamma=-\nabla p^{(1)}/\gamma \quad \text{(A4d)}$$

$$Re^{-1}\left[4\nabla\left(\nabla.\boldsymbol{u}\right)/3\right]=4Re^{-1}\nabla\left[\nabla.\left(M_b\boldsymbol{U}+\boldsymbol{u}^{(1)}\right)\right]/3=4Re^{-1}\nabla\left(\nabla.\boldsymbol{u}^{(1)}\right)/3 \quad \text{(A4e)}$$

$$-Re^{-1}\nabla\times\left(\nabla\times\boldsymbol{u}\right)=-Re^{-1}\nabla\times\left[\nabla\times\left(M_b\boldsymbol{U}+\boldsymbol{u}^{(1)}\right)\right]=-Re^{-1}M_b\nabla\times\left(\nabla\times\boldsymbol{U}\right)-Re^{-1}\nabla\times\left(\nabla\times\boldsymbol{u}^{(1)}\right) \quad \text{(A4f)}$$

Adding up Eqs. (A4a-f), we realize that the zero order terms yield back Eq. (9) associated with the steady field. Collecting terms to the first order in the wave amplitude, and disregarding smaller terms, we obtain

$$\partial\boldsymbol{u}^{(1)}/\partial t+M_b\boldsymbol{U}.\nabla\boldsymbol{u}^{(1)}+M_b\boldsymbol{u}^{(1)}.\nabla\boldsymbol{U}=-\nabla p^{(1)}/\gamma+4Re^{-1}\nabla\left(\nabla.\boldsymbol{u}^{(1)}\right)/3-Re^{-1}\nabla\times\left(\nabla\times\boldsymbol{u}^{(1)}\right) \quad \text{(A5)}$$

which by making use of the vector identity,

$$\left(\boldsymbol{U}.\nabla\right)\boldsymbol{u}^{(1)}+\left(\boldsymbol{u}^{(1)}.\nabla\right)\boldsymbol{U}=\nabla\left(\boldsymbol{u}^{(1)}.\boldsymbol{U}\right)-\boldsymbol{u}^{(1)}\times\left(\nabla\times\boldsymbol{U}\right)-\boldsymbol{U}\times\left(\nabla\times\boldsymbol{u}^{(1)}\right) \quad \text{(A6)}$$

leads to the leading-order, time-dependent momentum equation, referred to in Sec. III as Eq. (12).

References

[1]Uchida, S., "The Pulsating Viscous Flow Superposed on the Steady Laminar Motion of Incompressible Fluid in a Circular Pipe," *Journal of Applied Mathematics and Physics,* Vol. 7, 1956, pp. 403-422.

[2]White, F. M., *Viscous Fluid Flow*, McGraw-Hill Book Company Inc., New York, 1991, pp. 135-136.

[3]Majdalani, J., and Van Moorhem, W. K., "Improved Time-Dependent Flowfield Solution for Solid Rocket Motors," *AIAA Journal,* Vol. 36, No. 2, 1998, pp. 241-248.

[4]Brown, R. S., Blackner, A. M., Willoughby, P. G., and Dunlap, R., "Coupling Between Acoustic Velocity Oscillations and Solid Propellant Combustion," *Journal of Propulsion and Power,* Vol. 2, No. 5, 1986, pp. 428-437.

[5]Ma, Y., "A Simulation of the Flow Near a Burning Propellant in a Solid Propellant Rocket Motor," Ph.D. Dissertation, University of Utah, 1990.

[6]Barron, J., "The Onset of Turbulence in a Simulation of the Oscillating Flow Over a Burning Propellant," Ph.D. Dissertation, University of Utah, 1997.

[7]Van Dyke, M., *Perturbation Methods in Fluid Mechanics*, The Parabolic Press, Stanford, CA, 1975.

[8]Shaeffer, C. W., and Brown, R. S., "Oscillatory Internal Flow Studies," Chemical Systems Div. Rept. 2060 FR, United Technologies, San Jose, CA, Aug. 1992.

[9]Culick, F. E. C., "Rotational Axisymmetric Mean Flow and Damping of Acoustic Waves in a Solid Propellant Rocket," *AIAA Journal,* Vol. 4, No. 8, 1966, pp. 1462-1464.

[10]Lagerstrom, P. A., *Theory of Laminar Flows*, Section B, edited by F. K. Moore, Princeton University Press, Princeton, NJ, 1964.

[11]Chu, B. T., and Kovásznay, L. S. G., "Nonlinear Interactions in a Viscous Heat-Conducting Compressible Gas," *Journal of Fluid Mechanics,* Vol. 3, 1957, pp. 494-514.

[12]Carrier, B. T., and Carlson, F. D., "On the Propagation of Small Disturbances in a Moving Compressible Fluid," *Quarterly of Applied Mathematics,* Vol. 4, No. 1, 1946, pp. 1-12.

[13]Flandro, G. A., "Effects of Vorticity on Rocket Combustion Stability," *Journal of Propulsion and Power,* Vol. 11, No. 4, 1995, pp. 607-625.

[14]Majdalani, J., "A Hybrid Multiple Scale Procedure for Boundary Layers Involving Several Dissimilar Scales," *Journal of Applied Mathematics and Physics,* Vol. 49, No. 6, 1998.

[15]Butcher, J. C., The Numerical Analysis of Ordinary Differential Equations, Runge-Kutta and General Linear Methods, John Wiley & Sons, Great Britain, 1987, pp. 206-207.